Heliyon 10 (2024) e32361

Contents lists available at ScienceDirect

Heliyon

journal homepage: www.cell.com/heliyon

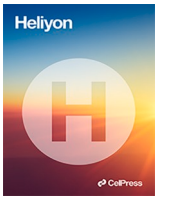

Research article

A multifunctional triboelectric nanogenerator based on PDMS/MXene for bio-mechanical energy harvesting and volleyball training monitoring

Renwei Yang

Ministry of Public Foundation, Shanghai University of Finance and Economics, Zhejiang College, 321013, Jinhua, China

ARTICLE INFO

Keywords:
Triboelectric nanogenerators (TENGs)
Self-powered sensor
PDMS/MXene
Volleyball training

ABSTRACT

Within the domain of wearable devices that are self-powered and sensory, triboelectric nanogenerators (TENGs) have surfaced as a notable solution to meet the growing needs for energy harvesting. This study unveils an innovative wearable and stretchable multifunctional double-layered TENG, based on PDMS/MXene, known as PM-TENG. Furthermore, PM-TENG can also be used as a joint sensor to monitor the movement of athletes' joints during volleyball training. By augmenting the matrix with PDMS/MXene, which possesses dual capabilities—namely, charge capture and charge movement—the intermediary layer is integrated. This leads to a two fold increase in the ability to trap charges and the overall triboelectric performance. With a power density reaching 11.27 mW, it notably exceeds the performance of its counterparts that solely utilize PDMS, by nearly 11 times. This academic effort elucidates the important role of PM-TENG in biomechanical energy capture and autonomous wearable sports motion sensing.

1. Introduction

The rapid development of multifunctional wearable technologies has brought unprecedented convenience into our daily lives [1]. This era is defined by the widespread use of the Internet of Things (IoTs), robotics, and artificial intelligence, enabling collaboration between humans and machines, personalized health assessments, and insights derived from data analytics [2,3]. Consequently, there is a growing demand for portable, flexible, stretchable, wearable gadgets that can function independently [4]. Conventional power storage systems, such as lithium-ion batteries and capacitors, struggle to meet power demands [5,6]. Their need for frequent recharging or replacement limits their functionality [7]. Consequently, the quest for enduring power sources intensifies, positioning energy harvesting modalities as potential game-changers. In the modern energy landscape, triboelectric nanogenerators (TENGs) stand out as champions of self-powered mechanisms that combine tribo-electrification and electrostatic induction to transform ambient mechanical energy into electrical energy [8–22]. TENGs, as emerging power generators, have numerous advantages: lightweight design, cost-effectiveness, versatility in material options, simple architecture, and impressive power density, to name a few [23–25]. The effectiveness of a TENG mainly revolves around the electrostatic induction capability and the charge trapping ability of its constituent materials [26].

A plethora of stratagems have been orchestrated to amplify TENG efficacy, encapsulating judicious material curation, surface engineering, and topological optimization [27]. In 2016, a significant advancement was made with the introduction of a functional layer designed to trap charges. This layer was strategically positioned between the triboelectric surface and its associated electrode

E-mail address: Z2012248@shufe-zj.edu.cn.

https://doi.org/10.1016/j.heliyon.2024.e32361
Received 15 February 2024; Received in revised form 3 June 2024; Accepted 3 June 2024
Available online 6 June 2024

[28]. This innovation highlighted its potential to enhance charge retention and subsequent energy generation. Improving the surface topography is crucial for increasing the TENG output. Predominantly, such alterations aim to magnify contact interfaces and augment surface irregularities. Thus, scholarly pursuits have dovetailed surface functionalization, electrostatic injections, microscopic structural craftsmanship, and composite material system genesis to realize formidable power densities. Lee and collaborators championed a C60-augmented TENG, setting new standards in output vigor [29]. Salauddin and team delineated the prowess of a sandpaper-aided micro-texture, uplifting the TENG output spectrum [30]. In another scholarly endeavor, Jae Park and associates unfurled a cation-enriched TENG, achieving amplified efficiency [31]. Yet, these technological marvels face inherent challenges: limited scalability, complex and costly production plans, vulnerability to aerial malfunctions, and compromised nano/microstructural durability. The alchemy of composite material selection, surface reengineering, and intermediary layer genesis emerges as the foundation to significantly enhance TENG performance, primarily by increasing surface charge densities. While strides have been made in performance enhancement, the elasticity and adaptability metrics necessitate further innovation, particularly with wearable paradigms in focus. The existing malleable TENG prototypes predominantly harness diverse electrodes, ranging from carbon nanotubes and carbonaceous pastes to graphene and silver nanowire conduits [32–34].

The search for electrodes that can be highly stretchable while maintaining excellent conductivity is difficult. This is because conductivity often decreases or disappears when the electrodes are under a lot of strain. To address these challenges, using knitted conductive fiber or yarn electrodes could be a potential solution for creating skin-like TENGs for wearable electronics in the future. When one integrates nanomaterials, including entities like MXene and graphene into polymer-based architectures, there's an enhancement in the intrinsic qualities of the resultant composite and a refinement of its surface characteristics [35–37]. Such an integration strategy has increasingly been recognized as an effective technique to amplify the efficacy of TENGs. As a result, the utilization of MXene as a dynamic nanofiller holds potential to transform composite materials tailored for top-performing TENGs. The proposal of charge storage layers has the potential to solve the problem of triboelectric charge dissipation [38,39]. Relevant studies have shown that charge storage layers can effectively avoid environmental interference, as charges are stored in closed compartments [40,41]. Additionally, TENG devices should be extended to sports monitoring equipment to achieve the practical application goals of TENG.

Our team has pioneered the creation of a double-layered triboelectric nanogenerator called PM-TENG, based on polydimethylsiloxane (PDMS)/MXene. This device integrates a PDMS film and PDMS/MXene composite film, offering flexibility, stretchability, water resistance, and heightened sensitivity. The PM-TENG is well-suited for wearable bio-mechanical energy harvesting and advanced sensor technology. The use of MXene was strategically employed to enhance the electronegativity of the tribolayer. This was accomplished by incorporating it with a large internal surface area, which was intricately adorned with oxygen groups carrying a negative charge. This introduction resulted in an increase in the number of induced charges, a finding that was confirmed through comprehensive surface potential evaluations and detailed electrical profiling. Additionally, MXene's amalgamation with silicone was strategized to elevate bi-functionality, chiefly charge entrapment and charge mobility, leveraging its innate microscopic dipole and conductivity traits. Consequently, while PDMS plays the role of a charge initiator, PDMS/MXene morphs into a bi-functional intermediary. Positioned as an intermediary, this specific layer is adept at seizing the triboelectric charges that emanate from the active stratum. Furthermore, it serves as a barrier, preventing these charges from recombining with their oppositely charged counterparts. This mechanism is crucial for enhancing the performance of the TENG. In this work, we undertook systematic assessments of the TENG, focusing on parameters like output voltage, current density, and the dynamics of charge transfer. To achieve this, we designed the PM-TENG with charge storage layer for human mechanical energy harvesting and joint monitoring in volleyball training. The PM-TENG was found to be a self-powered bio-motion sensor that can be attached to various human anatomical sites. It can harness energy from different motions such as tapping, walking, running, and even during recreational activities like volleyball. In summary, the results of this study represent a significant advancement in the development of flexible, adaptive, and wearable platforms designed for bio-mechanical energy collection and autonomous sensing. These advances not only set the stage for future innovations in wearable electronics, but also open the door for sports training monitoring.

2. Experimental section

2.1. Materials

The PDMS stock solution were obtained from Shanghai Kaiyin Chemical Co., Ltd. The conductive aluminum foils and Nylon films were bought from shopping mall. The LiF was procured from Shenzhen Rongchang Weiye Technology Co., Ltd. The hydrochloric acid (HCl, 35 %) solution was obtained from Kaifeng Shengyuan Chemical Co., Ltd. The Ti_3AlC_2 powder was bought from Beijing Deke Island Gold Technology Co., Ltd.

2.2. Conductiveation of the MXene powder

Usually, MXene nanosheets are prepared by stripping Ti_3AlC_2 as the etchant. Specifically, dissolve 2 g of LiF in 40 mL of 9 M hydrochloric acid while stirring in a glass for 6 min. Then, add 4 g of Ti_3AlC_2 powder to the solution, adjust the speed of the magnetic stirrer to 1000 rpm, and stir for 26 h at a temperature of 40 °C. Then, clean the mixture until the pH of the solution reaches 6. Then, the precipitate is added to deionized water and dispersed in the water through ultrasonic treatment. Finally, the supernatant of the solution was collected and subjected to vacuum freezing and drying to obtain the flaky MXene.

2.3. Conductiveation of the PDMS film and PDMS/MXene film

Mix the PDMS preparation solution with a mass ratio of 10:1 and prepare PDMS thin films using a spin coating apparatus. MXene powder was dispersed in ethanol through ultrasonic treatment for 45 min. Then, mix the MXene solution with the solution of PDMS and mix it evenly through ultrasonic treatment to prepare a mixed colloid with a weight concentration range of MXene. Next, add the curing agent to the mixed colloid and perform magnetic stirring for 15 min. The PDMS/MXene film with different thicknesses was prepared by spin coating.

2.4. Characterization and measurement

The TENG's output voltage was measured using a digital oscilloscope (SDS1202X–C). A low noise current preamplifier (model SR570) was utilized to monitor the current density. For tracking the transferred charge signals, an electrometer Keithley 6514 was employed. A self-made linear motor is used to provide the power required for TENG operation.

3. Results and discussion

Fig. 1(a1-a3) illustrate the conductiveation process of flaky MXene, and the inset shows the molecular structure of MXene. Fig. 1(b) shows the material structure configuration of PM-TENG. PM-TENG is architectured with a dual-layered design: a triboelectric layer composed of PDMS and a combined charge storage layer of PDMS/MXene. For electrodes, conductive aluminum foil are employed. Owing to its excellent electron capture ability, the PDMS layer predominantly functions as the triboelectric layer. In this particular layer responsible for generating charges, the phenomenon of triboelectricity occurs, resulting in the production of charges. These charges are then directed towards the conductive electrode layer through the presence of an electric field. Once in the conductive electrode layer, they combine with the opposing induced charges. The aforementioned phenomenon has the ability to hinder the excessive buildup of triboelectric charges within the region responsible for generating the charge, hence potentially reducing the effectiveness of the TENG's output. We've innovated a distinctive charge storage layer, which has been tactically positioned intermediately between the layers responsible for charge generation and collection. The primary role of this layer is to ensnare charges produced by the charge-generating stratum, thereby ensuring both the longevity and consistency of the triboelectric charges. Within

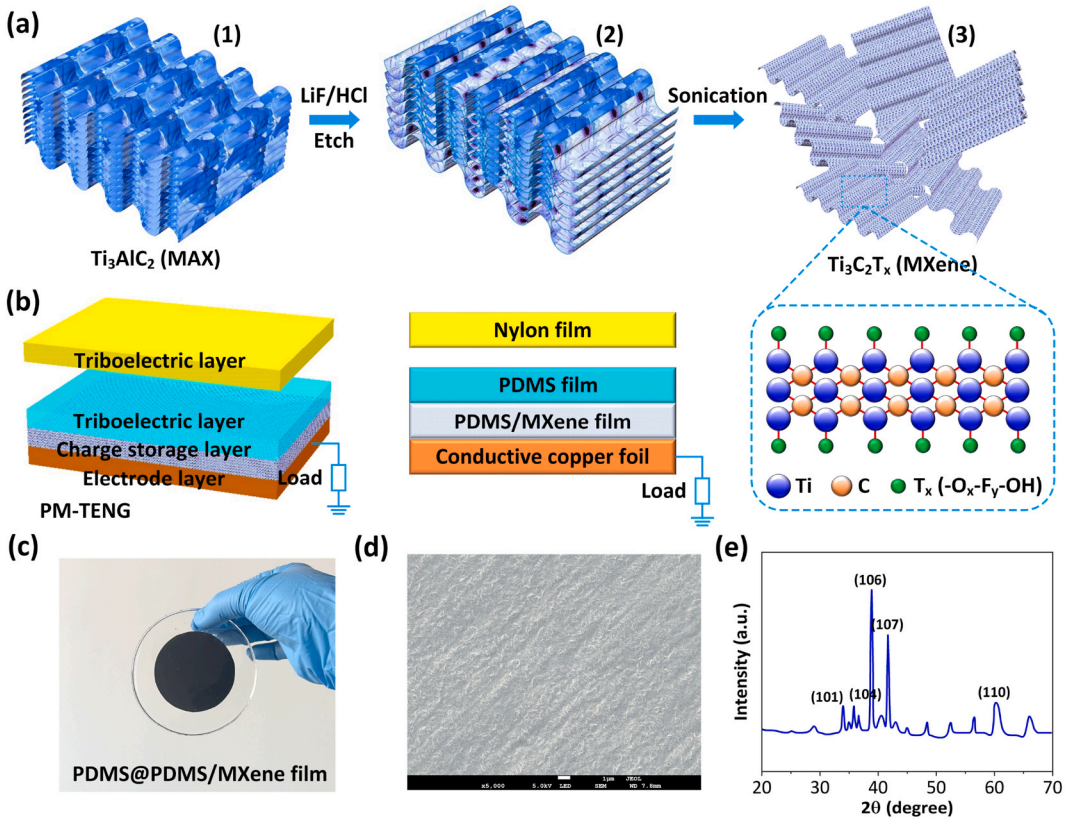

Fig. 1. (a1-a3) The preparation process of MXene powder. (b) Schematic diagram of PM-TENG's structural configuration. (c) The picture of PDMS@PDMS/MXene film. (d) The SEM image of PDMS/MXene film. (e) The XRD patterns of MXene powder.

this entrapment layer, the intrinsic properties of MXene, characterized by high electronegativity and a propensity to assimilate a profusion of electrons via functional groups, contribute significantly to the enhanced output of TENG. Owing to the inception of microcapacitors, this charge storage layer is adept at confining an elevated volume of surface charges on the PDMS/MXene composite, subsequently refining TENG's output. The conceptualization of the microcapacitor arises when proximate MXene fillers are separated by an ultra-thin dielectric barrier. This slender dielectric partition accentuates the microcapacitor's role in capacitive functionality, culminating in an elevated dielectric coefficient. Drawing from the tenets of the microcapacitor paradigm, introducing MXene into the PDMS polymer matrix augments its dielectric attributes and the TENG's surface charge density through the proliferation of micro-capacitors. Additionally, the MXene facilitates enhanced ion movement, thereby bolstering the conductivity quotient of the PDMS/MXene composite. Ascribed to its multifaceted functionalities, the PDMS/MXene amalgamation serves dually as a charge entrapment and transmission domain. Fig. 1(c) shows the picture of PDMS@PDMS/MXene film, and the surface texture features of PDMS@PDMS/MXene film was illustrated in SEM image from Fig. 1(d). As shown in Fig. 1(e), the XRD pattern of the MXene has three prominent peaks at 38°, 42°, and 61°, which correspond to the (106), (107), and (110) planes of $Ti_3C_2T_x$, which confirms the successful layering of the MXene.

Fig. 2(a and b) delineates the variations in dielectric constants for PDMS/MXene layers subjected to distinct MXene concentrations. The presence of numerous microcapacitors results in an escalation of the dielectric constant for PDMS/MXene from an initial value of 2.6–7.2. Notably, as the concentration of MXene increases to 4 % within the PDMS/MXene nanocomposites, there's a corresponding monotonic rise in the dielectric constant, thereby magnifying the composite layer's capacitance and facilitating augmented charge accumulation during contact electrification. Contrastingly, a surge in MXene's concentration within the PDMS matrix from 4 % to 6 % culminates in a dielectric constant decline, a phenomenon triggered by the undue aggregation of MXene, forming conductive pathways. Such behavior can be rationalized under the percolation theory framework. When the MXene concentration exceeds its percolation threshold, leakage current pathways emerge, stemming from the direct interfacing of neighboring MXene entities. As a result, the zenith of the dielectric constant is observed when the MXene concentration reaches a benchmark of 4 %. This specific concentration is identified as the optimal level, ensuring the highest effectiveness of the composite layer. To further substantiate the aforementioned dielectric constant effects, the surface potential was assessed at a separation of 2.5 mm for disparate filler proportions. One must duly acknowledge that there exists a direct association between the metrics of surface potential and electronegativity. This

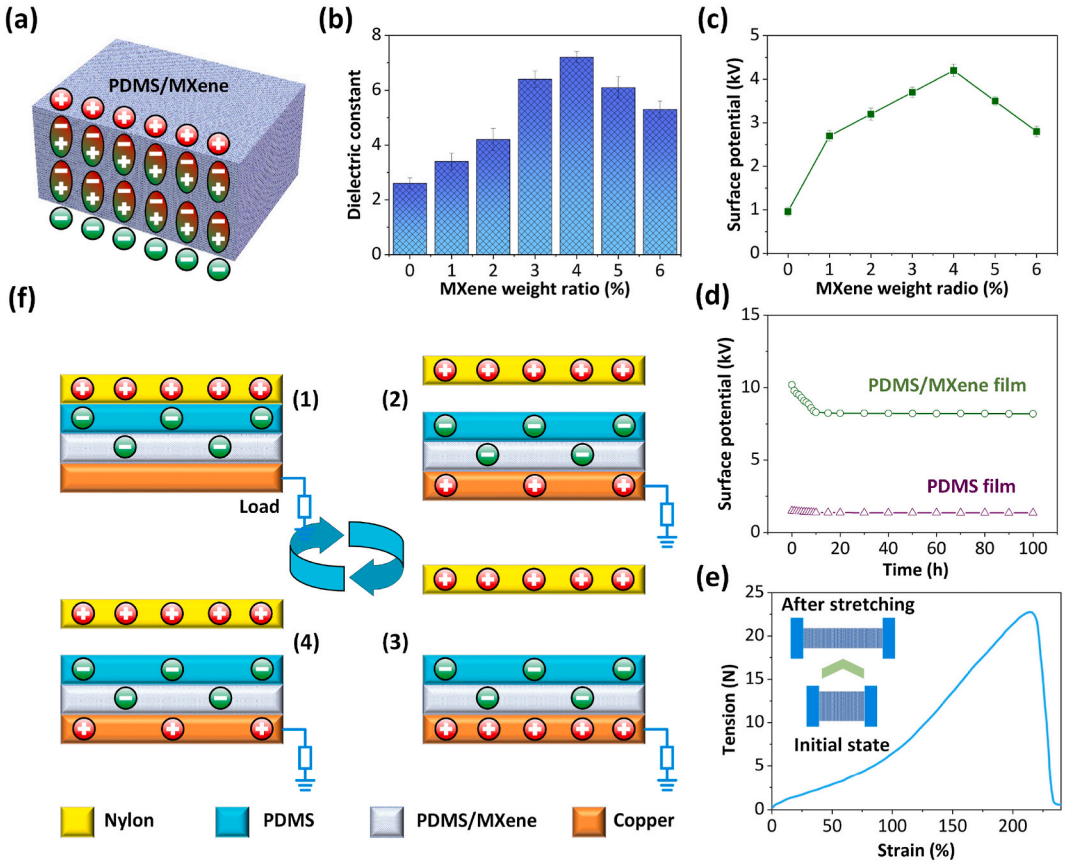

Fig. 2. (a) Schematic diagram of the working mechanism of the charge storage layer. (b) The dielectric constant of PDMS/MXene film with various MXene weight radio. (c) The surface potential of PDMS/MXene film with various MXene weight radio. (d) The surface potential comparison of PDMS/MXene film and PDMS film. (e) The stress-strain curve of the PDMS/MXene film. (f1-f4) The working mechanism of PM-TENG device.

electronegativity is intrinsically linked to the charge density that gets induced in the triboelectric layers. In this context, Fig. 2(c) illustrates the surface potentials for PDMS/MXene composites subjected to varying MXene concentrations post 60 contact electrification cycles. A zenith in surface potential is attained at 4.2 kV for PDMS/MXene with the integration of 4 % MXene, marking a fourfold increase relative to unadulterated PDMS. A detailed examination can be found in Fig. 2(d), which delineates the metrics related to the decay of surface potential. This decay is observed when subjected to mild hand taps and spans various materials including the singular PDMS layer and the PDMS/MXene layer. In the environment of a single nanocomposite layer, the triboelectric charges generated from the PDMS/MXene interface are trapped within shallow recesses. This makes them vulnerable to combining with electrode-induced charges and airborne ions, resulting in significant charge loss and a notable increase in surface potential decline. It's noteworthy that the dielectric constant exhibited by the PDMS/MXene layer stands at 7.2. Flexibly designed TENGs seamlessly integrate with the human body, adapting to various mechanical distortions in everyday situations. Enhancing stretchability not only augments wearable electronic device efficacy in capturing vital physiological metrics but also elevates wearer comfort. In light of this, uniaxial tension was deployed to gauge the as-conductiveated PM-TENG device's mechanical parameters, specifically stress and strain. This evaluation is graphically represented via the stress-strain curve in Fig. 2(e). Figs. S1(a and b) in Supplementary Materials show modulus and fracture toughness of PM-TENG with different MXene weight radios. The operational mechanism of the PM-TENG, illustrated in Fig. 2(f)–is predicated upon the synergistic interplay between tribo-electrification and the principles of electrostatic induction. As the PDMS/MXene triboelectric layer interacts with a nylon film, it accrues negative triboelectric charges, a phenomenon attributable to its intrinsic negative tribopolarity. In tandem, the nylon becomes laden with positive charges, as can be observed in Fig. 2(f1). In the subsequent phase, when a spatial gap ensues between the nylon and the PDMS/MXene layer, the conductive electrode responds to the triboelectric charges. It does so by generating corresponding negative electrostatic charges. This manifestation instigates a potential gradient, thereby compelling electrons to traverse from the conductive electrode towards the

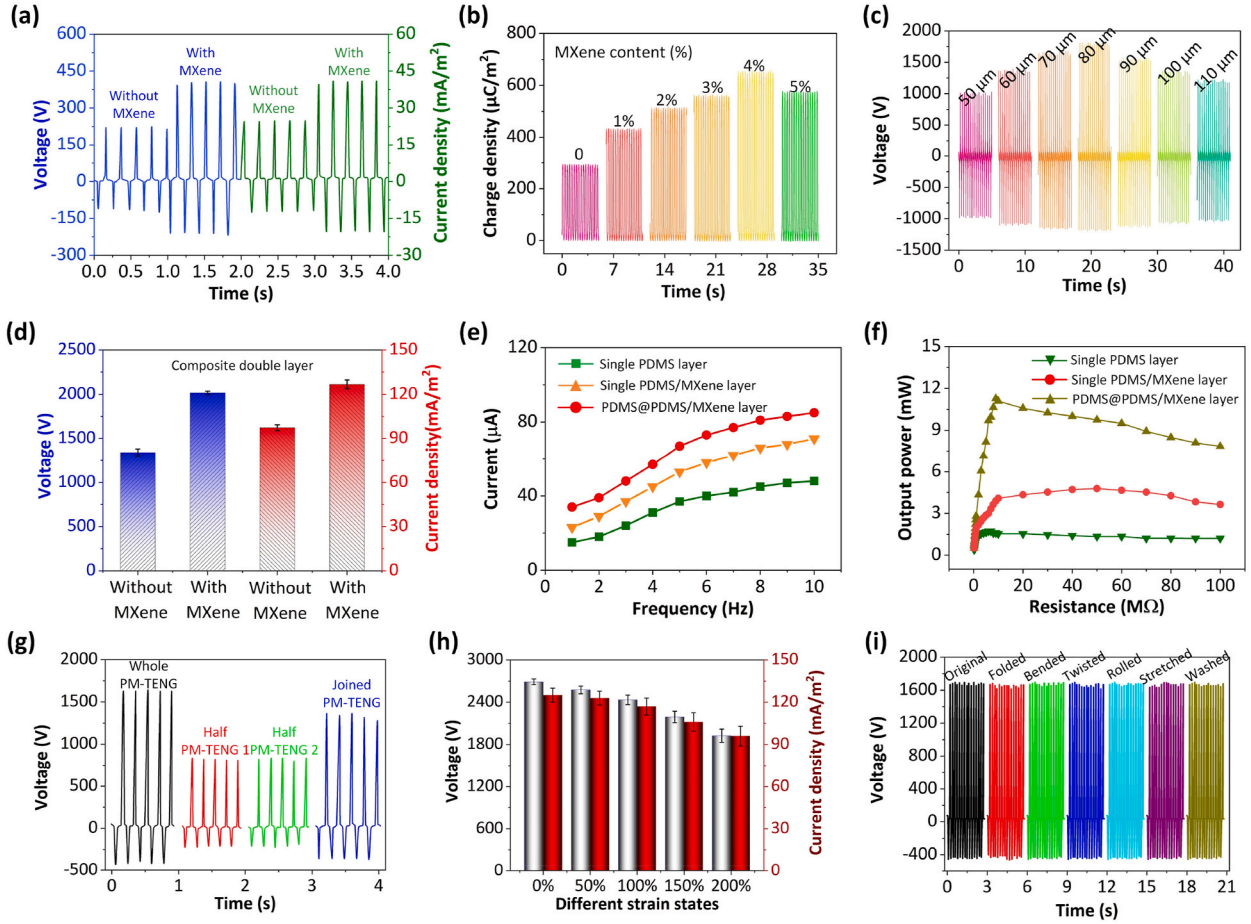

Fig. 3. (a) The output voltage and current of TENG based on the PDMS film with MXene and without MXene. (b) The charge density of PM-TENG with MXene weight ratio. (c) The influence of PDMS/MXene film on the PM-TENG. (d) The electrical output of PM-TENG based on composite double layer with MXene and without MXene. (e) The influence of working frequency on output voltage/current of PM-TENG based on different film combinations. (f) The output power of PM-TENG based on different film combinations. (g) Comparison of the output voltages of the PM-TENG in the original, half-cut, and joined devices. (h) The output voltage and current of PM-TENG under different strain states. (i) The influence of various extreme deformations on PM-TENG output performance.

grounding via the external circuit, as depicted in Fig. 2(f2). Such an electron flow endures up to the point where the maximum spatial separation between the materials is realized, as shown in Fig. 2(f3). On the contrary, when the nylon re-approaches the PDMS/MXene interface, the profusion of positive charges on the conductive electrode starts waning. This triggers a reversal in electron movement: they now embark on a journey from the grounding back to the electrode. This process perpetuates until a complete reunion of the two surfaces is accomplished, as described in Fig. 2(f4). This recurring contact-separation dynamic enables the PM-TENG to perpetually yield an alternating current.

Fig. 3(a) shows the influence of MXene on output performance of PM-TENG. According to results, the introduction of MXene will increase the triboelectric performance of PDMS, but the performance improvement effect is limited. As depicted in Fig. 3(b), the incorporation of MXene into the PDMS has discernible implications on the performance metrics of the TENG. Specifically, it sheds light on the evolving trends of voltage, current density, and the density of transferred charge as time progresses, all maintained under uniform experimental conditions. Variations in the concentration of MXene have a direct bearing on the observed profiles of both current density and the density of transferred charge. Introducing 4 % MXene into PDMS culminates in an optimal output, showing a remarkable elevation of over double when compared with the benchmark of undoped PDMS. The heightened output underscores the pivotal roles played by the formation of MXene microcapacitors and the presence of oxygen-functional groups in the TENG's tribo-electrification processes. Yet, a surge in MXene concentration from 4 % to 5 % inversely affects the TENG's output. Such diminution likely stems from excessive MXene agglomeration, subsequently curtailing the composite film's capacitance. Supporting observations emerge from dielectric constant and surface potential evaluations. Consequently, an ideal MXene concentration in PDMS is deduced to be 4 %. Fig. 3(c) visualizes how output voltage interplays with the thickness of PDMS/MXene. Excessively thin films instigate a leakage current trajectory, neutralizing triboelectric and induced charges, thereby attenuating triboelectric outputs. The optimal voltage is obtained with a thickness around 1 mm. Such an optimal film thickness elevates insulating resistance, negating leakage currents and thereby optimizing output. However, films exceeding this optimal thickness yield a reduced power output attributed to diminished charge quantities. Subsequent evaluations thus leveraged this 1 mm optimal thickness. Building upon the insights gleaned from earlier research endeavors, an intermediate layer composed of a 80 μm thickness PDMS/MXene composite film was judiciously selected to optimize the TENG's output. An increment in the thickness of this intermediate layer naturally culminates in enhanced charge entrapment capabilities, a direct consequence of an increasingly populated trap milieu. Fig. 3(d) captures the output metrics of the PM-TENG, both with and devoid of the MXene nanofiller, under specified conditions. Without the presence of MXene as a nanofiller, the output metrics of the PM-TENG register at roughly 1344 V and 97.5 mA/m^2. However, introducing MXene into the equation elevates these output figures, catapulting them to 2016 V and 126.66 mA/m^2. Within the architectural construct of the PM-TENG, the accentuated accumulation of negative charges by MXene translates to a superior triboelectric output, a phenomenon deeply rooted in the microscale dipole interactions. As a logical progression, ensuing characterizations predominantly harnessed the capabilities of the MXene-imbued PM-TENG. With an aspiration to fine-tune the PM-TENG's performance metrics, investigative endeavors pivoted towards understanding the ramifications of varying the PDMS/MXene layer's thickness and intricacies arising from alterations in the contact-separation frequency. Reportedly, triboelectric charge density nuances hinge on parameters such as surface potential, relative dielectric constants, and dielectric film thickness. Fig. 3 (e) illustrates the performance of single PDMS film, PDMS/MXene film, and PDMS@PDMS/MXene film across a frequency range from 1 Hz to 10 Hz. A vibration shaker facilitated these frequency adjustments. Findings indicate that as the input frequency escalates, the output concurrently amplifies, with peak outputs observed for the combined MXene layer configuration. The observed amplification can be ascribed to the heightened contact-separation frequency, enhancing the electrode's charge transfer rate. The versatility in material choice remains a cardinal advantage of TENGs. Evidently, the choice of antithetical triboelectric layers profoundly impacts the resultant electrical yield. Thus, synergizing materials with contrasting tribopolarities offers promising avenues for bolstering the TENG output performance. Under a load resistance of 9 MΩ, the corresponding maximum output power of PM-TENG is about 11.27 mW, which is about 11 times that of pure PDMS TENG, as illustrated in Fig. 3(f). According to results in Figs. S2(a and b) of Supplementary Materials, when the mechanical frequency increases from 2 Hz to 10 Hz, the I_{sc} of PM-TENG will also increase, while the Q_{sc} of PM-TENG can remain stable. According to results in Figs. S2(c and d) of Supplementary Materials), when the force applied to PM-TENG increases, the I_{sc} and Q_{sc} of PM-TENG also increase. The PM-TENG exhibits superior electrical output capabilities and offers easy customization, facilitating the design of fashionable apparel. Our research endeavors delved into scrutinizing the output voltage, spanning diverse configurations of the PM-TENG, encompassing the complete apparatus, the bifurcated half-cut device-1, its counterpart half-cut device-2, and the subsequently amalgamated device, as vividly illustrated in Fig. 3(g). Intriguingly, in the cases of both the half-cut device-1 and half-cut device-2, their output voltages resonate with roughly half the magnitude observed for the output of the undivided device. Rejoining the two sections of the energy-generating unit allows it to nearly recover its original output voltage, revealing only a 15 % reduction. Notably, even after division into separate units, the device maintains its fundamental functionality. Such modifiability is crucial as it facilitates the production of TENG-integrated apparel in diverse sizes and designs. Owing to its remarkable attributes of flexibility and stretchability, the PM-TENG is capacitated to generate salient electrical impulses, particularly when operationalized at a frequency resonance of 5 Hz. We secured the PM-TENG's ends using two clamps and mounted it on a linear motor to maintain consistent contact with a nylon film. As illustrated in Fig. 3(h)–a linear decline in output voltage is observed as the stretching length of the PM-TENG increases from 0 to 200 %. A discernible decrement is observed in the output voltage, which transitions from an initial 2016 V to a subsequent 1452 V. This decremental trajectory can be primarily ascribed to the attenuation of the dielectric layer's thickness combined with a diminished conductivity exhibited by the intricately knitted fabric electrode in the stretched state of the PM-TENG. For wearable technology applications, the PM-TENG's flexibility and resilience are critical attributes. Hence, we examined the PM-TENG's output performance under various mechanical deformations and wash conditions. As illuminated in Fig. 3(i), the PM-TENG's electrical outputs exhibit no significant variations when the device is exposed to a myriad of mechanical manipulations, inclusive of actions like bending, twisting,

rolling, and the rigorous process of washing. To evaluate the device's resilience, its performance was meticulously gauged by administering gentle taps, both before and subsequent to its subjection to the aforementioned mechanical strains. Notably, the meticulously crafted PM-TENG invariably produces a steadfast voltage, maintaining its consistency even after undergoing multiple deformation cycles. According to results in Fig. S3(a) of Supplementary Materials, the environment temperature has almost no influence on PM-TENG output. However, when the relative humidity in the environment increases, the output performance of PM-TENG first decreases and then stabilizes, as shown in Fig. S3(b) of Supplementary Materials. This is because as relative humidity rises, the triboelectric charges of PM-TENG will experience a loss. However, the charge in the storage layer will not experience a loss due to being in a closed environment. Hence, as the relative humidity continues to rise, the output performance of PM-TENG remains stable.

Fig. 4(a) serves as an illuminating guide, presenting a side-by-side comparison of the power densities harvested by the PM-TENG across a spectrum of biomechanical movements. The device showcases its prowess across various operational modes, reaching zenith power densities-for instance, a staggering 12.48 W/m^2 from the act of a three-finger tap, as meticulously cataloged in our findings. Among the repertoire of biomechanical actions, the triumvirate tap of three fingers emerges as the most bountiful, registering the pinnacle of energy outputs. Building on this revelation, our study pivoted towards exploiting the PM-TENG's capability. We embarked on a mission to extract biomechanical energy stemming from the rhythmic taps of fingers, with an endgame to transpose this harvested energy into a tangible power source for wearable electronics. Furthermore, we charge a 1 μF capacitor via PM-TENG driven by jumping, running, and walking, as shown in Fig. 4(b). The energy stored in capacitor can arrive at 22.56 μJ, 79.65 μJ, and 440.74 μJ, respectively, as illustrated in Fig. 4(c). Augmenting its portfolio of applications, as Fig. 4(d) delineates, the PM-TENG, when strategically embedded within shoes, proves adept at capturing and converting energy from a spectrum of human motions, be it the rhythmic cadence of a run or the explosive burst of a jump. Among the cataloged human motions, the act of jumping, contingent on the intricacies of the exerted force and frequency, stands out, registering the pinnacle of voltage outputs. To robustly assess its durability and sustained performance, the PM-TENG was subjected to an extended operational test. In this comprehensive analysis, the PM-TENG's output voltage was consistently monitored across a staggering 36,000 cycles. This was done by exposing the device to a consistent compressive load of 10 N, oscillating at a frequency of 3 Hz. Fig. 4(e) vividly captures the tenacity of the PM-TENG, showcasing its unwavering voltage output amidst numerous compressions.

Expanding the application of PM-TENG in the field of sports training is very meaningful. As shown in Fig. 5(a), volleyball players undergo a series of movements in various joints of their bodies during training, therefore monitoring various joints of the body plays an important role in assisting training. For the commencement of our exploratory analysis, the PM-TENG module was judiciously aligned on the external facade of a phalangeal joint. In the context of cyclical finger flexure, the apparatus manifested a distinguishable and unwavering voltage waveform, lucidly illustrated in Fig. 5(b). Subsequent to the PM-TENG's adhesion to the wrist region, a congruous physiological waveform emerged, vividly represented in Fig. 5(c). An extended scrutiny entailed the strategic placement of the PM-TENG on both the cubital and femoral articulations. This facilitated the acquisition of pertinent electrical outputs, as substantiated in Fig. 5(d and e), respectively.

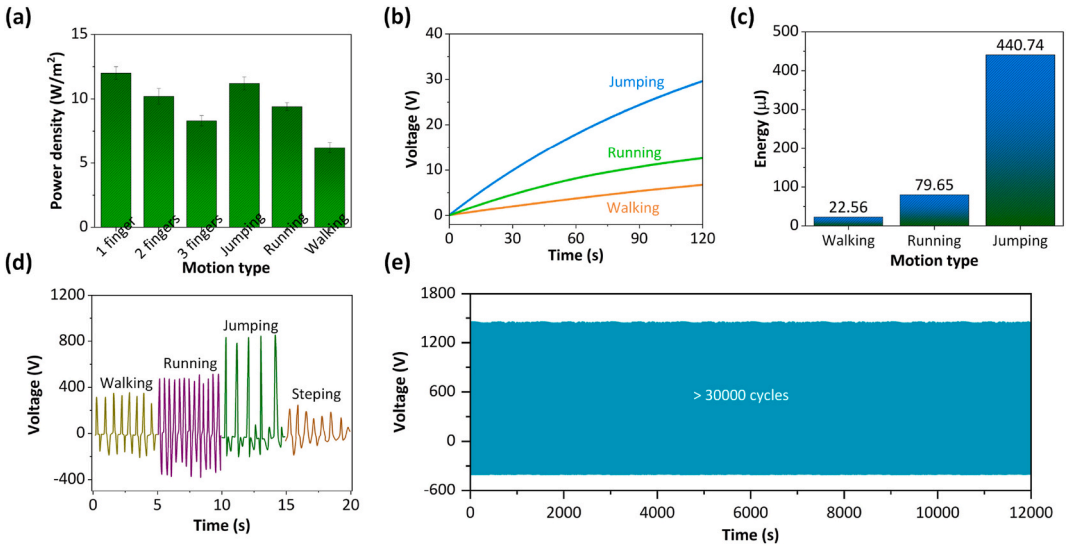

Fig. 4. (a) The output power density of PM-TENG under various human motion. (b) The charging curves of 1 μF capacitor using the PM-TENG driven by jumping, running, and walking. (c) The storage energy in 1 μF capacitor using the PM-TENG driven by jumping, running, and walking. (d) The output signal of PM-TENG under walking, running, jumping, and steping. (e) The output stability test of PM-TENG under more than 30000 consecutive working conditions.

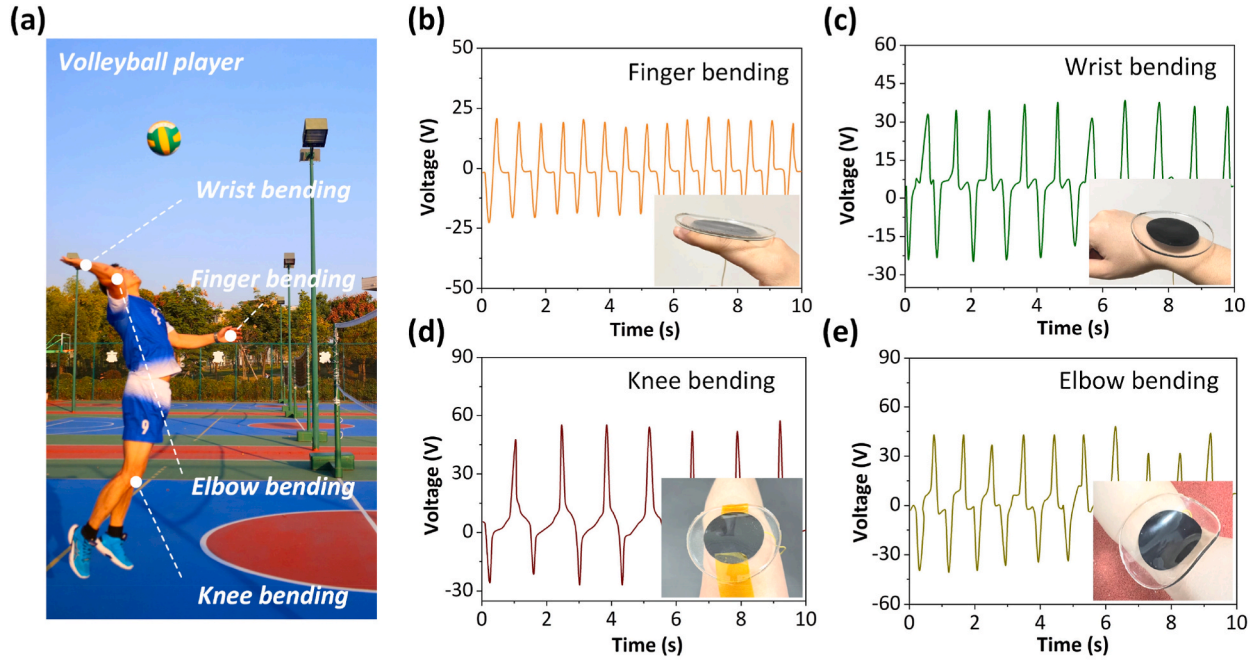

Fig. 5. (a) Photograph of volleyball player undergoing volleyball training. (b–e) The output signal of PM-TENG installed on various joints of the body, including finger, wrist, knee, and elbow.

4. Conclusion

In summary, the PDMS film and PDMS/MXene film were designed to fulfill a dual role: charge generation and the augmentation of the PM-TENG efficacy. Furthermore, the inclusion of MXene-renowned for its charge trapping and transportation prowess-within the silicone bolstered the film's charge retention and electronegativity competencies. The resulting outcome indicated a significant nine-fold improvement, mainly due to the introduction of micro-capacitor structures and the increase in electrical conductivity. This intermediate layer efficiently reduces the buildup of triboelectric charges, enhancing the PM-TENG's performance. Under a load resistance of 9 MΩ, the corresponding maximum output power of PM-TENG is about 11.27 mW, which is about 11 times that of pure PDMS TENG. Moreover, PM-TENG can monitor the movement of volleyball players by sensing human joints. The inherent advantages of PM-TENG have been utilized, highlighting its versatility in various mechanical energy collection modes, including autonomous biological motion sensing, for example, in the field of sports motion sensing.

Data availability statements

Data available on request from the authors.

CRediT authorship contribution statement

Renwei Yang: Writing – review & editing, Writing – original draft, Visualization, Validation, Supervision, Software, Resources, Project administration, Methodology, Investigation, Funding acquisition, Formal analysis, Data curation, Conceptualization.

Declaration of competing interest

The authors declare that they have not known competing financial interests or personal relationships that could have appeared to influence the work reported in this study.

Appendix A. Supplementary data

Supplementary data to this article can be found online at https://doi.org/10.1016/j.heliyon.2024.e32361.

References

[1] T. Dinh, T. Nguyen, H.P. Phan, et al., Stretchable respiration sensors: advanced designs and multifunctional platforms for wearable physiological monitoring, Biosens. Bioelectron. 166 (2020) 112460.
[2] C. Zhang, Y. Lu, Study on artificial intelligence: the state of the art and future prospects, Journal of Industrial Information Integration 23 (2021) 100224.
[3] H. Wang, T. Fu, Y. Du, et al., Scientific discovery in the age of artificial intelligence, Nature 620 (7972) (2023) 47–60.
[4] J.P. Bharadiya, A comparative study of business intelligence and artificial intelligence with big data analytics, American Journal of Artificial Intelligence 7 (1) (2023) 24.
[5] M.B.F. Ahsan, S. Mekhilef, T.K. Soon, et al., Lithium-ion battery and supercapacitor-based hybrid energy storage system for electric vehicle applications: a review, Int. J. Energy Res. 46 (14) (2022) 19826–19854.
[6] M. Ibrahim, M.G. Fayed, S.G. Mohamed, et al., High-performance lithium-ion battery and supercapacitors using covalent organic frameworks (COFs)/Graphitic carbon Nitride (g-C3N4)-derived hierarchical N-doped carbon, ACS Appl. Energy Mater. 5 (10) (2022) 12828–12836.
[7] X. Gao, J. Yang, Z. Xu, et al., Recent progress of aqueous and organic/aqueous hybrid electrolytes for low-temperature rechargeable metal-ion batteries and supercapacitors, Energy Storage Mater. 54 (2023) 382–402.
[8] J. Luo, W. Gao, Z.L. Wang, The triboelectric nanogenerator as an innovative technology toward intelligent sports, Adv. Mater. 33 (17) (2021) 2004178.
[9] W.G. Kim, D.W. Kim, I.W. Tcho, et al., Triboelectric nanogenerator: structure, mechanism, and applications, ACS Nano 15 (1) (2021) 258–287.
[10] Y. Zou, J. Xu, K. Chen, et al., Advances in nanostructures for high-performance triboelectric nanogenerators, Advanced Materials Technologies 6 (3) (2021) 2000916.
[11] T. Cheng, Q. Gao, Z.L. Wang, The current development and future outlook of triboelectric nanogenerators: a survey of literature, Advanced Materials Technologies 4 (3) (2019) 1800588.
[12] Z. Zhao, L. Zhou, S. Li, et al., Selection rules of triboelectric materials for direct-current triboelectric nanogenerator, Nat. Commun. 12 (1) (2021) 4686.
[13] W. Liu, Z. Wang, G. Wang, et al., Integrated charge excitation triboelectric nanogenerator, Nat. Commun. 10 (1) (2019) 1426.
[14] R. Dharmasena, S.R.P. Silva, Towards optimized triboelectric nanogenerators, Nano Energy 62 (2019) 530–549.
[15] J. Luo, Z.L. Wang, Recent progress of triboelectric nanogenerators: from fundamental theory to practical applications, EcoMat 2 (4) (2020) e12059.
[16] Y. Zhou, M. Shen, X. Cui, et al., Triboelectric nanogenerator based self-powered sensor for artificial intelligence, Nano Energy 84 (2021) 105887.
[17] Z.L. Wang, Triboelectric nanogenerator (TENG)—sparking an energy and sensor revolution, Adv. Energy Mater. 10 (17) (2020) 2000137.
[18] Y. Zhou, W. Deng, J. Xu, et al., Engineering materials at the nanoscale for triboelectric nanogenerators, Cell Reports Physical Science 1 (8) (2020).
[19] G. Khandelwal, N.P.M.J. Raj, S.J. Kim, Triboelectric nanogenerator for healthcare and biomedical applications, Nano Today 33 (2020) 100882.
[20] S.A. Lone, K.C. Lim, K. Kaswan, et al., Recent advancements for improving the performance of triboelectric nanogenerator devices, Nano Energy 99 (2022) 107318.
[21] B. Cheng, Q. Xu, Y. Ding, et al., High performance temperature difference triboelectric nanogenerator, Nat. Commun. 12 (1) (2021) 4782.
[22] B. Cheng, Q. Xu, Y. Ding, et al., High performance temperature difference triboelectric nanogenerator, Nat. Commun. 12 (1) (2021) 4782.
[23] W. Liu, Z. Wang, C. Hu, Advanced designs for output improvement of triboelectric nanogenerator system, Mater. Today 45 (2021) 93–119.
[24] C. Zhang, Y. Liu, B. Zhang, et al., Harvesting wind energy by a triboelectric nanogenerator for an intelligent high-speed train system, ACS Energy Lett. 6 (4) (2021) 1490–1499.
[25] Y. Zou, V. Raveendran, J. Chen, Wearable triboelectric nanogenerators for biomechanical energy harvesting, Nano Energy 77 (2020) 105303.
[26] X. Wei, Z. Zhao, C. Zhang, et al., All-weather droplet-based triboelectric nanogenerator for wave energy harvesting, ACS Nano 15 (8) (2021) 13200–13208.
[27] X. Li, C. Zhang, Y. Gao, et al., A highly efficient constant-voltage triboelectric nanogenerator, Energy Environ. Sci. 15 (3) (2022) 1334–1345.
[28] X. Xin, X. Chen, C. Zhao, et al., Intermediate layer for enhanced triboelectric nanogenerator, Nano Energy 79 (2021) 105439.
[29] G.H. Han, S.H. Lee, J. Gao, et al., Sustainable charged composites with amphiphobic surfaces for harsh environment–tolerant non-contact mode triboelectric nanogenerators, Nano Energy 112 (2023) 108428.
[30] M. Salauddin, S.M.S. Rana, M.T. Rahman, et al., Fabric-assisted MXene/silicone nanocomposite-based triboelectric nanogenerators for self-powered sensors and wearable electronics, Adv. Funct. Mater. 32 (5) (2022) 2107143.
[31] S.M.S. Rana, M.T. Rahman, S. Sharma, et al., Cation functionalized nylon composite nanofibrous mat as a highly positive friction layer for robust, high output triboelectric nanogenerators and self-powered sensors, Nano Energy 88 (2021) 106300.
[32] H. Wang, M. Shi, K. Zhu, et al., High performance triboelectric nanogenerators with aligned carbon nanotubes, Nanoscale 8 (43) (2016) 18489–18494.
[33] S. Kim, M.K. Gupta, K.Y. Lee, et al., Transparent flexible graphene triboelectric nanogenerators, Adv. Mater. 26 (23) (2014) 3918–3925.
[34] M.G. Stanford, J.T. Li, Y. Chyan, et al., Laser-induced graphene triboelectric nanogenerators, ACS Nano 13 (6) (2019) 7166–7174.
[35] Q. Jiang, C. Wu, Z. Wang, et al., MXene electrochemical microsupercapacitor integrated with triboelectric nanogenerator as a wearable self-charging power unit, Nano Energy 45 (2018) 266–272.
[36] H. Chen, Y. Xu, L. Bai, et al., Crumpled graphene triboelectric nanogenerators: smaller devices with higher output performance, Advanced Materials Technologies 2 (6) (2017) 1700044.
[37] Wen He, et al., Flexible single-electrode triboelectric nanogenerators with MXene/PDMS composite film for biomechanical motion sensors, Nano Energy 78 (2020) 105383.
[38] SM Sohel Rana, et al., Metal-organic framework and molybdenum oxide doped highly negative hybridized triboelectric material for self-powered and continuous monitoring of biosignals, Chem. Eng. J. 473 (2023) 144989.
[39] SM Sohel Rana, et al., Cobalt-nanoporous carbon functionalized nanocomposite-based triboelectric nanogenerator for contactless and sustainable self-powered sensor systems, Adv. Funct. Mater. 31 (52) (2021) 2105110.
[40] M. Toyabur Rahman, et al., Silicone-incorporated nanoporous cobalt oxide and MXene nanocomposite-coated stretchable fabric for wearable triboelectric nanogenerator and self-powered sensing applications, Nano Energy 100 (2022) 107454.
[41] SM Sohel Rana, et al., Zirconium metal-organic framework and hybridized Co-NPC@ MXene nanocomposite-coated fabric for stretchable, humidity-resistant triboelectric nanogenerators and self-powered tactile sensors, Nano Energy 104 (2022) 107931.